Fault Analysis of Midchannel Power Takeoff in Diagonal Conducting Wall Magnetohydrodynamic Generators

Motoo Ishikawa*
Kyoto University, Kyoto, Japan
and
Y.C.L. Wu† and M.H. Scott‡
The University of Tennessee Space Institute, Tullahoma, Tennessee

The effects of loading faults on the midchannel power takeoff of a diagonal conducting wall magnetohydrodynamic generator are investigated. The fault analysis considers loading schemes for connecting multiple external loads to the channel. It is shown that applying the concept of diodes in series with power takeoff electrodes as implemented in the end regions is harmful or ineffective for the midchannel power takeoff, since it may trigger premature faults or cause the multiple loading to be ineffective. It is also shown that faults can be treated in the same manner as other off-design conditions in the power takeoff of the end region. Two-dimensional calculations show that an open-circuit condition in the upstream load circuit results in a large current density at power takeoff anodes accompanied by a shorting current over the interframe insulators at the cathode. A short-circuit condition in the upstream load circuit causes a large current density at the power takeoff cathodes and drives a shorting current at the anode.

Introduction

MULTIPLE loads will be needed for large-scale diagonal generators since it is difficult to maintain local optimum loading throughout a long channel with a single load[1] and the capacity of inverters is limited. Multiple loading points, in turn, require that electrode frames in the midportion of the channel be used to interface with the external load. The configuration of the external load when multiple loads are required may take the form where each section of the channel has its own independent load. This is referred to as the direct coupling loading scheme.[1] Under normal circumstances the current in each of these loads is coupled only to the plasma current flowing in that corresponding section of the generator.

Alternatively, more complicated circuitry can be used that couples the plasma current in the various sections of the channel through the loads; i.e., part of the plasma current from one channel section passes through more than one loading section. This scheme is referred to as the indirect or feedback coupling scheme[1] and is generally characterized by all loads terminating at a common point at one end of the channel. The other ends for each load section terminate at an appropriate potential at various locations in the channel. In contrast, the loads of the direct scheme appear in series.

The design and operation of the power takeoff (PTO) for diagonal-type magnetohydrodynamic (MHD) generators have been investigated experimentally in the University of Tennessee Space Institute (UTSI) diagonal conducting wall (DCW) channel,[1,2] the U-25B channel,[3] and the AVCO Mark VI channel,[4] among others. Analytical studies have been published by Levi,[5] Pan and Doss,[6,7] Ishikawa and Wu,[8] Ishikawa et al.,[9] and others, that primarily concentrated on the end region where the fringing magnetic field distorts the electrical field.

At UTSI, both the direct and indirect (feedback coupling) power takeoff schemes were investigated[1]; in the U-25B and the Chinese channels the usual midchannel PTO schemes for direct coupling were examined[3,10]; and a mixed direct and indirect power takeoff scheme was studied in U-25 channels.[11] It has been demonstrated that an increased electrical power is generated with multiple vs single loads even in small channels. Analytical works were carried out by several researchers such as Levi,[5] Pan and Doss,[6,7] and Yoshida and Umoto.[12] A large difference of power output was predicted between single- and multiload channels in large-scale generators.[12]

In the end regions, faults occurring in the load circuits can be treated as any other off-design condition and can be controlled by adequate design considerations of the power takeoff. On the other hand, in the midchannel region, the power takeoff must maintain a balance of load currents, particularly for the direct coupling scheme. If the balance is broken by faults in the load circuits, very large currents will flow at the small number of midchannel frames designated for power takeoff. The large currents can cause channel damage.

The following sections describe the loading schemes considered and discuss the implications of loading faults. The current distribution in a small-scale device (28 MW_t) is presented to illustrate the fault effects. Similar behavior can also be predicted for large-scale devices with the potential for severity of damage increasing with size (i.e., load current).

Basic Considerations of Midchannel Power Takeoff

Investigations of the PTO behavior and its effects on generator performance have been primarily concerned with the end regions where the fringing magnetic field complicates current and potential distributions. Relatively little attention has been given to the midchannel power takeoff region because it is easy to treat in small generators. It should be noted, however, that additional factors need to be considered when investigating the midchannel PTO behavior, particularly in load circuit faults and the applicability of diodes. A schematic view of the midchannel power takeoff region for a DCW MHD generator is given in Fig. 1 along

Presented as Paper 82-0922 at the AIAA 20th Aerospace Sciences Meeting, Orlando, FL, Jan. 11-14, 1982; received June 6, 1982; revision received March 6, 1985. This paper is declared a work of the U.S. Government and therefore is in the public domain.

*Associate Professor, Department of Electrical Engineering.
†Professor and Administrator, Energy Conversion Research and Development Programs. Associate Fellow AIAA.
‡Manager, Gasdynamics Section, Energy Conversion Research and Development Programs.

with the coordinate system used in the two-dimensional calculations. In this figure, I_1 and I_2 are the load current in the front and rear sections, respectively. The corresponding load resistances are R_{L1} and R_{L2}. Other parameters shown in the figure are s, the frame pitch; h, the duct height in the y direction; u, the velocity of plasma; B, the magnetic field; θ, the diagonal angle; and x, y, and z, the reference coordinates.

Midchannel PTO Schemes

Four basic configurations, shown schematically in Fig. 2, for the midchannel PTO will be discussed here. The first three are examples of directly coupled loading. The fourth is an indirect or feedback coupling scheme. The first configuration, illustrated in Fig. 2a, utilizes connection to only one electrode frame. This scheme is presented for simplicity in performing the two-dimensional calculations. Extension of the investigation to plural PTO frames schemes is, however, not difficult.

The separate PTO scheme, illustrated in Fig. 2b, splits the midchannel PTO region into two regions. This scheme will not be discussed further herein as it is obviously of no practical interest. It is introduced because all other schemes can be modeled, to some extent, by superimposing the separated regions.

The third scheme, shown in Fig. 2c, uses multiple PTO frames for directly coupled external loads. This configuration is required for real channels. Diodes included here will be shown later to be either harmful or ineffective for the midchannel power takeoff.

The fourth scheme (see Fig. 2d) is applicable when the external loads are configured into what is referred to as the feedback loading scheme. This scheme as well as the direct coupling scheme were investigated experimentally at UTSI.[1] The basic equations and features were discussed in Ref. 1. In this paper only the simplest case is discussed for clarity. In Fig. 2d, R_{L1} and R_{L2} are the load resistances, I_1 and I_2 the load currents, V_{o1} and V_{o2} the open-circuit voltages, and R_{i1} and R_{i2} the internal resistances. The following relations are derived:

$$I_1 = \frac{(R_{L2}+R_{i2})\ V_{o1} + R_{L2}\ V_{o2}}{(R_{L1}+R_{i1})\ (R_{L2}+R_{i2}) + R_{L2}\ R_{i2}} \tag{1}$$

$$I_2 = \frac{(R_{L1}+R_{i1})\ V_{o2} - R_{i2}\ V_{o1}}{(R_{L1}+R_{i1})\ (R_{L2}+R_{i2}) + R_{L2}\ R_{i2}} \tag{2}$$

In general, the outermost load current I_1 will be somewhat larger than that of the second by an amount proportional to the difference in short-circuit currents of the two channel portions.

Fault Analysis—Direct Coupling

In this paper, the term "fault" is used to describe events in the channel's external load circuit, such as the occurrence of an open circuit or short circuit in the load rather than applying to local faults such as a breakdown between adjacent frames which is the usual connotation.

In end regions, it has been observed experimentally that operation at load current levels near the short-circuit condition caused current concentrations at the innermost PTO frames located closest to the external load.[2] This behavior was well predicted numerically by a two-dimensional electrodynamic analysis.[8] As the external load moves toward an open-circuit condition there is a small effect in the end PTO regions since the magnitude of open-circuit voltage is small there. Thus, loading faults can be treated as off-design conditions in the end PTO regions. However, this is not true within the main generating region.

On the other hand, in the midchannel PTO region there is a possibility of a severe current overload when faults occur. The number of midchannel PTO frames is expected to be much less than that of end PTO frames in the direct coupling scheme because of the balanced current during normal operation. However, the number required will increase with the size of the device since the current increases accordingly. These frames must carry the current difference between the two load circuits. A balance between the magnitude of these two load currents must be maintained. A short- or open-circuit condition for one load circuit alters the balance and presents the potential for frame damage and effects on the plasma flow such as shocks or flow separation.

Open- and short-circuit fault conditions are illustrated in Fig. 3 for the single PTO frame. When the load in the upstream circuit, R_{L1}, becomes open, the total load current I_2 must flow from the anode of the midchannel PTO frame into the plasma. This will result in high current densities at this anode.

When the load of the upstream circuit, R_{L1}, becomes shorted the difference between two load currents, $(I_{\text{short}} - I_2)$, must flow out of the plasma through the cathode. The magnitude of this current is similar to that of the open-circuit condition discussed above since $I_{\text{short}} \simeq 2I_2$. The cases for open- and short-circuit conditions for the downstream load circuit R_{L2} are similar to the cases of the short- and

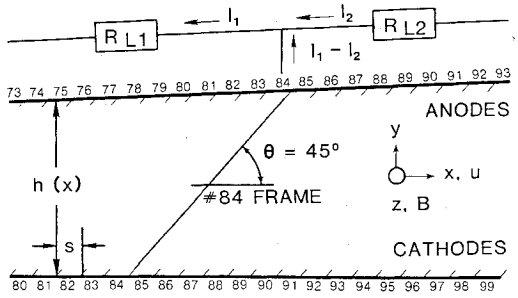

Fig. 1 Schematic of the midchannel power takeoff region and coordinate system.

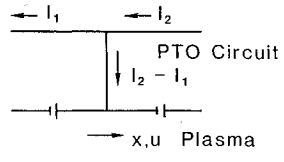

a) Single power takeoff frame.

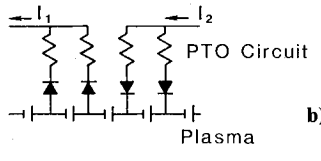

b) Separated power takeoff frames.

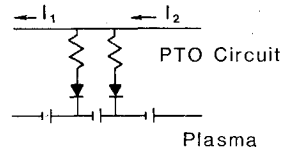

c) Plural power takeoff frames.

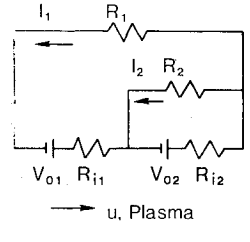

d) Feedback coupling scheme.

Fig. 2 Schematic for the midchannel power takeoff configurations considered.

open-circuit conditions, respectively, of the upstream load circuit, R_{L1}.

The configuration that has multiple frames connected with diodes is now considered. The possible faults are illustrated in Fig. 4. With diodes removed from the circuit, the behavior at fault conditions is essentially the same as for the single PTO frame scheme. However, in this case, the current is distributed among several frames. The diodes, however, introduce a complication to the behavior pattern. When the downstream load circuit R_{L2} moves toward the short-circuit condition with the direction of diodes shown in Fig. 4, the current $I_2 - I_1$ flows out of the plasma through the anodes of the PTO frames. If, on the other hand, the load circuit R_{L1} moves toward the short-circuit condition, a point is reached where the diodes block the current flow. In essence, this eliminates the midchannel power takeoff and creates the situation where the channel becomes connected to a single load, as shown in Fig. 4b.

For an open-circuit condition in the load circuit R_{L2}, the diodes again prevent the current from flowing and force the other load circuit, R_{L2}, to the open condition as well (Fig. 4c). Thus, the entire generator is brought to the open-circuit condition.

If the load circuit R_{L1} becomes open, the current I_2 flows to the anodes of the PTO frames. The direction of the diodes as shown (Fig. 4d) will not interfere with the current flow.

Over the range of operation, the possibility exists that the sign of the term $I_1 - I_2$ will change. The use of diodes will only allow current to flow in one direction which makes the multiple loading only partially effective.

a) R_{L1}: open. b) R_{L1}: short.

Fig. 3 Schematic showing the fault currents considered for the single power takeoff frame.

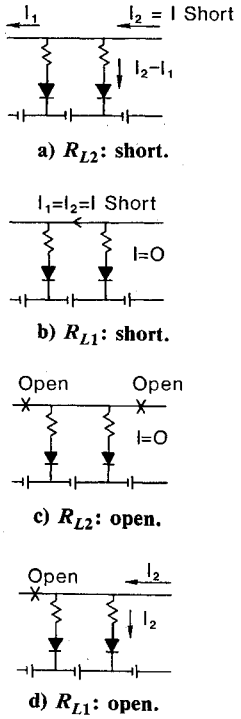

a) R_{L2}: short.

b) R_{L1}: short.

c) R_{L2}: open.

d) R_{L1}: open.

Fig. 4 Schematic showing fault currents when diodes are included.

In summary, possible faults in load circuits create adverse conditions that provide a potential source for damage to the midchannel PTO region of the direct coupling loading scheme, therefore, appropriate protection devices should be designed in the load circuits.

Fault Analysis—Feedback Coupling

For the second type of external loading scheme (illustrated in Fig. 2d)—feedback coupling—four possible faults are considered. It is assumed that $R_{L1} = R$, $R_{L2} = 3R$, $R_{i1} = R_{i2} = R_i$, and $V_{o1} = V_{o2} = V_o$ for simplicity.

1) $R_{L1} = 0$ or short

$$I_1 = V_o/R_i \qquad I_2 = 0$$

2) $R_{L1} = \infty$ or open

$$I_1 = 0 \qquad I_2 = \frac{V_o}{3R + R_i}$$

3) $R_{L2} = 0$ or short

$$I_1 = \frac{V_o}{R + R_i} \qquad I_2 = \frac{RV_o}{R_i(R + R_i)} = \frac{V_o}{R_i} - I_1$$

4) $R_{L2} = \infty$ or open

$$I_1 = \frac{2V_o}{R + 2R_i} \qquad I_2 = 0$$

The most severe of these possible faults is a short for the second load (i.e., $R_{L2} = 0$). Other faults result in currents that change from nominal conditions by a factor on the order of 2 at most. Under normal conditions most of the generator current flows through the outer load loop (I_1). The current through the second load increases the current in the downstream half of the channel by an amount considered proportional to the difference in short-circuit current be-

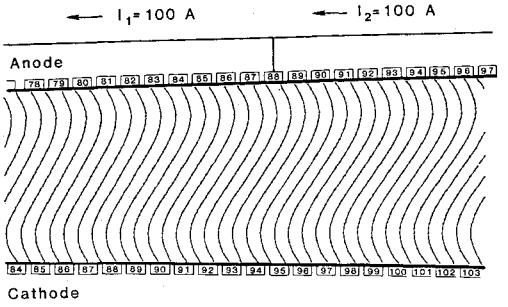

Fig. 5 Current distribution for the reference case.

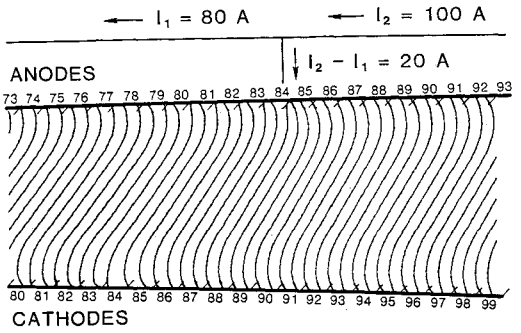

Fig. 6 Current distribution for a current imbalance ($I_2 - I_1$) of 20 A.

tween the two channel portions. When the second load resistance becomes shorted, a much larger current will flow. This current can be an order of magnitude greater than that for nominal conditions.

Two-Dimensional Calculations

Two-dimensional calculations are carried out for the low mass flow (LMF) channel to be run in the Department of Energy Coal-Fired Flow Facility (CFFF) at the University of Tennessee Space Institute.

Basic Equations and Numerical Procedure

The basic electrodynamic equations are Maxwell's equations and the generalized Ohm's law. With introduction of the current stream function ψ, the following differential equation is obtained:

$$\frac{\partial^2\psi}{\partial x^2}+\frac{\partial^2\psi}{\partial y^2}+\left(\sigma\frac{\partial}{\partial x}\frac{1}{\sigma}-\frac{\partial}{\partial y}\frac{\beta}{\sigma}\right)\frac{\partial\psi}{\partial x}$$
$$+\sigma\left(\frac{\partial}{\partial x}\frac{\beta}{\sigma}+\frac{\partial}{\partial y}\frac{1}{\sigma}\right)\frac{\partial\psi}{\partial y}-\sigma\frac{\partial}{\partial x}(uB)=0 \qquad (3)$$

The integration of Eq. (3) along the z direction yields

$$\frac{\partial^2\psi'}{\partial x^2}+\frac{\partial^2\psi'}{\partial y^2}+\left(\sigma\frac{\partial}{\partial x}\frac{1}{\sigma}-\frac{\partial}{\partial y}\frac{\beta}{\sigma}\right)\frac{\partial\psi'}{\partial x}$$
$$+\sigma\left(\frac{\partial}{\partial x}\frac{\beta}{\sigma}+\frac{\partial}{\partial y}\frac{1}{\sigma}\right)\frac{\partial\psi'}{\partial y}-\frac{\sigma}{I}\frac{\partial}{\partial x}(uBw)=0 \qquad (4)$$

where

$$\psi'=\psi\, w(x)/I \qquad (5)$$

and I is the reference current, $w(x)$ the duct width along the z direction, σ the electrical conductivity, and β the Hall parameter. The boundary conditions for Eq. (4) are that electrodes are equipotential surfaces and normal current density vanishes on insulators.[8] In addition, for a DCW channel, current is conserved and the corresponding cathodes and anodes are at the same potential.

For the gasdynamic portion of the solutions, the core flow and boundary-layer thickness are calculated using a two-dimensional code.[14] The properties of the combustion gas plasma are calculated for Illinois No. 6 coal with flow rates corresponding to the nominal condition for the CFFF LMF channel. Gasdynamics and electrodynamics are not coupled in the present fault analysis since the interaction is relatively weak and the investigation is preliminary.

The parameters at the midchannel PTO are

$$X_0=148.4\text{ cm},\quad h_0=14.36\text{ cm},\quad w_0=11.75\text{ cm}$$
$$\theta=45\text{ deg},\quad B_0=3.2\text{ T},\quad u_0=1350\text{ m/s}$$
$$T_0=2580\text{ K},\quad P_0=1.20\text{ atm},\quad \delta_0=4.0\text{ cm}$$
$$\sigma_0=6.20\text{ mho/m},\quad \beta_0=1.3$$

where X_0 is the location of the PTO cathode, δ the boundary-layer thickness, h and w the height and width of the channel, respectively, and the subscript 0 refers to the core condition at the midchannel PTO electrode.

In the numerical procedures, the velocity and temperature distributions are given for calculations of the current stream function. A modified successive over-relaxation (SOR) method is applied with the second-order finite difference scheme. The details of the numerical procedures are reported in Refs. 8 and 13.

Current Distribution

The electrical calculations are carried out for the axial location corresponding to the region between anode 73 (and cathode 80) and anode 93 (and cathode 99), as illustrated in Fig. 1. Frame 84 is chosen as the PTO frame. The computations are made for the open- and short-circuit conditions at the load circuit R_{L1} (see Fig. 1) since the open-circuit condition of R_{L1} corresponds to the short-circuit condition of R_{L2} and vice versa.

The current distribution shown in Fig. 5 is used as in the reference and ideal cases. The load currents I_1 and I_2 are equal and there is no current flow at the PTO frame. The difference of the contours for the streamlines is 10 A in this and subsequent figures. A uniform current distribution is obtained.

The current distributions for the two unbalanced load cases: 1) $I_1=80$ A and $I_2=100$ A and 2) $I_1=40$ A and $I_2=100$ A, are shown in Figs. 6 and 7, respectively. A small current concentration at the PTO anode is seen in Fig. 6 as the load unbalance increases, a larger concentration at the PTO anode as well as the shorting current from cathodes 84 to 83 are shown in Fig. 7. A similar shorting current was

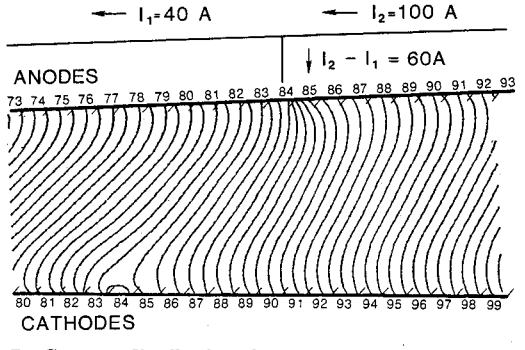

Fig. 7 Current distribution for a current imbalance (I_2-I_1) of 60 A.

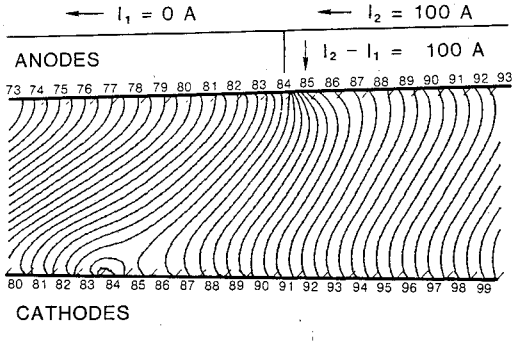

Fig. 8 Current distribution for the open-circuit (R_{L1}) fault condition.

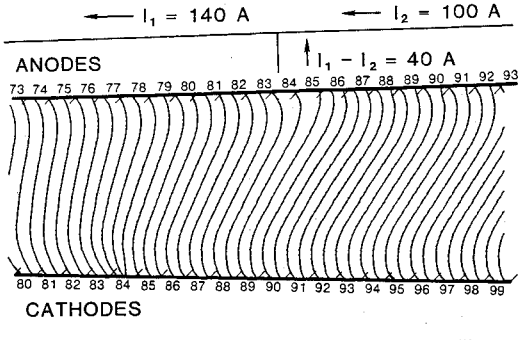

Fig. 9 Current distribution for a current imbalance (I_1-I_2) of 40 A (R_{L1} moving toward a short-circuit condition).

calculated and analyzed in the off-design conditions in the end PTO region.[9]

Figure 8 shows the current distribution in the fault case (open circuit) with $I_1 = 0$ and $I_2 = 100$ A. A large unbalanced current flows at the PTO anode and a large shorting current occurs from cathode 84 to the adjacent cathodes. The resulting large local Lorentz force may cause separation of the gas boundary layer at the cathode side.

The current distribution toward the short-circuited fault case is shown in Fig. 9 where $I_1 = 140$ A and $I_2 = 100$ A are considered. The difference of I_1 and I_2 should flow at the PTO cathode from the plasma into the PTO circuit. The current concentration is seen at cathode 84 and a slight disturbance of the current appears near the PTO anode (anode 84). Figure 10 depicts the current distribution for a more severe imbalance with $I_1 = 160$ A and $I_2 = 100$ A. The shorting occurs from anodes 84 to 85.

Electrical Stress at the PTO Electrodes

Table 1 shows the electrical stress (J_y^2/σ) at the power takeoff frame, obtained from the two-dimensional calculations.

For reference, the current density and the joule dissipation P_{joule} in the core regions are

$$J_x = -0.453 \text{ A/cm}^2, \quad J_y = -0.824 \text{ A/cm}^2$$

$$P_{\text{joule}} = (J_x^2 + J_y^2)/\sigma_0 = 14.3 \text{ W/cm}^3$$

In Table 1, the case of $I_1 - I_2 = 0$ represents the balanced load condition, while the negative and positive values of $I_1 - I_2$ correspond to the variation of loads R_{L1} and R_{L2} relative to the balanced loads. Negative values occur as R_{L1} increases toward open circuit and the PTO frame carries current out of the anode.

Figures 11 and 12 illustrate the electrical stress at the PTO anode and cathode, respectively. For the cases of the open-circuit conditions at R_{L1}, the PTO anode has a large current density and joule dissipation, as shown in Fig. 11. When $I_1 - I_2 = -100$ A, the values of J_y and P_{joule} are 3.7 and 13.9 times larger than those of the nominal case. In the short-circuit condition, the electrical stress at the PTO anode is reduced as compared with the nominal condition, but a shorting current occurs between anodes as shown in Figs. 7 and 8. Figure 12 shows that the PTO cathode experiences a large electrical stress for the short-circuit conditions of R_{L1}. When $I_1 - I_2 = 60$ A, the values of J_y and P_{joule} are 2.6 and 6.8 times larger than those of the nominal case. It is obvious that stresses can be reduced to tolerable levels if several frames are used in the midchannel PTO.

Table 2 illustrates the magnitudes of the current and the Lorentz force across the interframe insulator near the PTO frame that are representative of the maximum stress that can occur. Lower values can be obtained when multiple frames are employed.

The Lorentz force drives the current toward the core flow at the cathode side for the open-circuit conditions and at the

Table 1 Electrical stress at PTO frame

	Anode		Cathode	
$I_1 - I_2$, A	J_y, A/cm^2	J_y^2/σ, W/cm^3	J_y, A/cm^2	J_y^2/σ, W/cm^3
−100	−3.66	30.4	1.49	5.16
−80	−3.08	21.6	1.03	2.47
−60	−2.54	14.7	0.54	0.68
−40	−2.01	9.18	−0.03	0.00
−20	−1.56	5.53	−0.56	0.73
0	−0.98	2.18	−1.01	2.37
20	−0.49	0.55	−1.56	5.66
40	−0.005	0.00	−2.11	10.4
60	0.52	0.61	−2.62	16.0

Table 2 Current and Lorentz force over insulator

On cathode-side insulator (cathodes 84 to 83)
$I_1 - I_2 = -100$ A
$J_x = 1.09$ A/cm^2, $I_x^a = 18.9$ A
$J_x B = 3.50 \times 10^4$ N/m^3, $J_x^2/\sigma = 2.76$ W/cm^3
On anode-side insulator (anodes 84 to 85)
$I_1 - I_2 = 60$ A
$J_x = 0.282$ A/cm^2, $I_x^a = 4.0$ A
$J_x B = 0.90 \times 10^4$ N/m^3, $J_x^2/\sigma = 0.18$ W/cm^3

[a] I_x is the total shorting current over the interframe insulator.

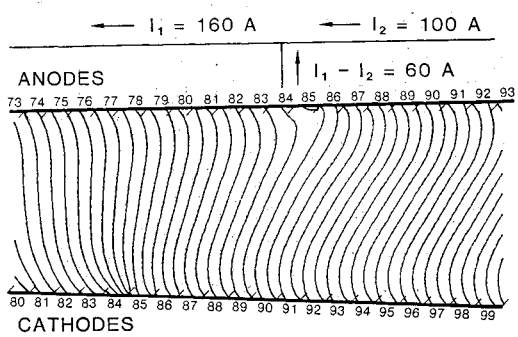

Fig. 10 Current distribution for a current imbalance ($I_1 - I_2$) of 60 A (R_{L1} moving toward a short-circuit condition).

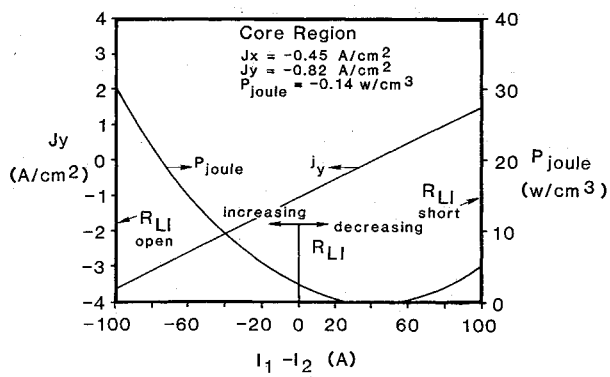

Fig. 11 Electrical stress at the power takeoff anode (frame 84).

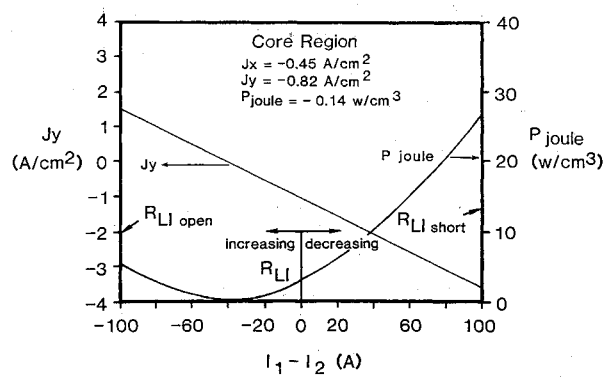

Fig. 12 Electrical stress at the power takeoff cathode (frame 84).

anode side for the short-circuit conditions. This may cause the boundary layer to separate. The joule dissipation over the interframe insulators is large enough to lead to the degradation of the insulators.

Calculations made with fully coupled electrical and gasdynamic equations are needed to understand the details of the faults. However, despite the limitations, the present analysis provides the qualitative understanding of faults in the midchannel PTO.

Conclusions

A preliminary analysis of the loading faults on the midchannel power takeoff (PTO) has been carried out. There is a potential for severe damage on channels caused by faults in the midchannel PTO region of the direct coupling loading scheme. In addition, the diodes, which are needed in the end regions, are either harmful or ineffective in the midchannel PTO of the direct coupling.

The two-dimensional calculations showed that the open-circuit condition of the upstream load circuit results in a large current density at the PTO anode and drives a shorting current over the interframe insulators at the cathode side. The short-circuit condition of the upstream load circuit results in a large current density at the PTO cathode and a shorting current over the interframe insulators at the anode side.

Acknowledgments

The gasdynamical parameters used herein were taken from a part of the calculation results for designs of the Coal-Fired Flow Facility Low Mass Flow channel carried out by John T. Lineberry. This work was supported by the U.S. Department of Energy under Contract DE-AC02-79ET10815.

References

[1]Muehlhauser, J. M. et al., "Experimental Investigation of Multiple-Loaded Diagonal Conducting Wall Generators," *Proceedings of the 16th Symposium on Engineering Aspects of Magnetohydrodynamics,* p. I.3, 1977.

[2]Galanga, F. L. et al., "Experimental Results of the UTSI Coal-Fired MHD Generator and Investigations of Various Power Take-off Schemes," AIAA Paper 81-0030, Jan. 1981.

[3]Rudins, G. et al., "A Study of the Operation of the U25B Facility MHD Generator Under Conditions of Strong Electric and Magnetic Field," *7th International Conference on MHD,* Vol. I, Cambridge, MA, June 1980, p. 1.

[4]Demirjian, A. M. and Duijano, I. M., "Power Conditioning and Control Requirements of Coal-Fired MHD Generators," AIAA Paper 81-0246, Jan. 1981.

[5]Levi, E., "Preliminary Design for the Power Take-Off of Single-Loaded Magnetohydrodynamics Channels," *Energy Conversion and Management*, Vol. 20, 1980, p. 33.

[6]Pan, Y. C. and Doss, E. D., "Power Take-Off Analysis for Diagonally Connected MHD Channels," AIAA Paper 80-0253, 1980.

[7]Pan, Y. C. and Doss, E. D., "Analyses of the Power Take-off Regions of the U25 Bypass and the US U-25 Channels," *7th International Conference on MHD*, Vol. I, Cambridge, MA, June 1980, p. 178.

[8]Ishikawa, M. and Wu, Y. C. L., "Two-Dimensional Analysis of Power Take-Off Region in Coal Fired MHD Generator and Comparison with Experiments," *Proceedings of the 19th Symposium on Engineering Aspects of Magnetohydrodynamics,* June 1981, p. 8.4.

[9]Ishikawa, M., Wu, Y. C. L., and Scott, M. H., "Analytical and Experimental Results of Two-Dimensional and Nonuniform Effects in Power Take-Off Region in UTSI Coal Fired MHD Generator," *1981 IEEE International Conference on Plasma Science,* May 1981, IEEE, New York, p. 19.

[10]Zi-Xiang, J. et al., "The Preliminary Experiments of the Coal-Preheated Air Combustion-Driven MHD Generation," *Proceedings of the 19th Symposium on Engineering Aspects of Magnetohydrodynamics,* June 1981, p. 1.2.

[11]Bityurin, V. A. et al., "Investigation of the "RM" Diagonal Channel on the U-25 Facility," *7th International Conference on MHD*, Vol. I, Cambridge, MA, June 1980, p. 69.

[12]Yoshida, M. and Umoto, J., "A New Quasi-Two-Dimensional Analysis of Whole Electrical and Gasdynamical Performances of Linearly-Diverging Diagonal-Type Generator," *7th International Conference on MHD,* Vol. II, Cambridge, MA, June 1980, p. 524.

[13]Ishikawa, M. and Wu, Y. C. L., "Two-Dimensional Effects in Power Take-Off Region," Topical Report for the U.S. Department of Energy, FE-10815-55, 1981.

[14]Lineberry, J. T. et al., "A Comparison of Experimental Results from the UTSI Coal-Fired MHD Generator to Theoretical Prediction," AIAA Paper 81-0031, Jan. 1981.